

Bergische Universität Wuppertal

Fakultät für Mathematik und Naturwissenschaften

Institute of Mathematical Modelling, Analysis and Computational Mathematics (IMACM)

Preprint BUW-IMACM 26/24

F. Kasolis, M. Clemens

A Nonlinear Port-Hamiltonian Transmission-Line Benchmark

November 3, 2026

http://www.imacm.uni-wuppertal.de



Preprint – Preprint – Preprint – Preprint – Preprint – Preprint

A Nonlinear Port-Hamiltonian Transmission-Line Benchmark

Fotios Kasolis
Department of Mathematics and Informatics
University of Wuppertal, Wuppertal, Germany
kasolis@uni-wuppertal.de

Markus Clemens
Chair of Electromagnetic Theory
University of Wuppertal, Wuppertal, Germany
clemens@uni-wuppertal.de

***Abstract*—We propose a nonlinear transmission line as a physically motivated and engineering-relevant benchmark problem for nonlinear port-Hamiltonian PDE-DAE systems and structure-preserving numerical methods. A soft ferromagnetic core introduces a current-dependent incremental inductance through a saturating magnetic constitutive relation, while a distributed memoryless nonlinear resistive shunt gives rise to an algebraic constraint. The resulting system possesses a rank-two descriptor matrix and a differentiation index of one. The strictly monotone shunt characteristic admits analytical inversion, yielding an equivalent two-state quasilinear PDE system. An exact power-balance identity provides a reference for assessing numerical dissipation, constraint preservation, and energy consistency.**

***Index Terms*—Nonlinear port-Hamiltonian systems, benchmark model, soft ferromagnetism, saturable permeability, index-one reduction.**

I. Introduction and Benchmark Motivation

Port-Hamiltonian (pH) systems provide an energy-based framework for modeling dynamical systems, explicitly capturing their interconnection structure, dissipation mechanisms, and boundary port interactions [1]. Their numerical treatment becomes particularly challenging when nonlinear constitutive relations coexist with singular descriptor operators and boundary power exchange. This motivates the development of benchmark problems with analytically verifiable structural properties, enabling systematic evaluation of numerical methods in terms of accuracy, constraint preservation, and energy consistency.

Here, we propose a nonlinear lossy transmission line as a benchmark for nonlinear pH PDE-DAE systems. Rather than aiming at a high-fidelity description of a particular physical device, the model is designed to combine mathematical tractability with physically interpretable constitutive mechanisms and engineering relevance. In contrast to the classical telegrapher equations [2], a soft-ferromagnetic core introduces a nonlinear magnetic constitutive relation, while a distributed memoryless nonlinear resistive shunt gives rise to an algebraic constraint. These idealized mechanisms yield a model combining state-dependent wave propagation, a singular descriptor matrix, an index-one algebraic structure, and an exact power-balance identity within a minimal one-dimensional setting.

Furthermore, the algebraic shunt current can be eliminated analytically, yielding an equivalent explicit PDE formulation. The availability of both PDE-DAE and reduced PDE representations, together with analytically verifiable structural properties, enables systematic benchmarking of numerical methods with respect to constraint preservation, energy consistency, numerical stability, and wave propagation accuracy.

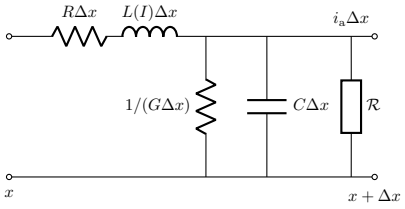


Fig. 1. Lumped-cell approximation of the nonlinear transmission line. The current-dependent inductance models magnetic saturation, while the nonlinear resistive shunt satisfies $V = \mathcal{R}(i_{\mathrm{a}})$.

II. Nonlinear Distributed Line Model

Consider a nonlinear transmission line with distributed equivalent lumped-cell circuit consisting of a linear series resistance, a nonlinear current-dependent inductance, a linear shunt conductance and capacitance, and an additional memoryless nonlinear resistive shunt, as depicted in Fig. 1. The transmission line occupies the spatial interval $x \in (0, \ell)$, with time $t \geq 0$. Let I and V denote the line current and voltage, respectively, and let i_{a} be the current per unit length drawn by a distributed nonlinear shunt. The line parameters per unit length are the series resistance $R \geq 0$, shunt conductance $G \geq 0$, and capacitance $C > 0$. The current-dependent incremental inductance $L(I)$ is assumed to satisfy

$$0 < L_{\min} \leq L(I) \leq L_{\max} < \infty. \tag{1}$$

The inductive nonlinearity emerges from magnetic saturation in a soft ferromagnetic core. Adopting a simplified reversible, memoryless approximation of the nonlinear B-H characteristic [3], we consider

$$B(H) = \mu_{\mathrm{s}} H + (\mu_{\mathrm{i}} - \mu_{\mathrm{s}}) H_* \tanh(H/H_*), \tag{2}$$

where B and H denote the magnetic flux density and field intensity, respectively, $H_* > 0$ is a characteristic saturation field, and $\mu_{\mathrm{i}} > \mu_{\mathrm{s}} > 0$ are the initial and limiting differential

Preprint – Preprint – Preprint – Preprint – Preprint – Preprint

permeabilities. Differentiation yields

$$\mu_{\mathrm{diff}}(H) = \frac{dB}{dH} = \mu_{\mathrm{s}} + (\mu_{\mathrm{i}} - \mu_{\mathrm{s}})\,\mathrm{sech}^2(H/H_*). \quad (3)$$

Assuming a fixed magnetic geometry, negligible leakage flux, and a spatially uniform effective magnetic field, we set $H = \kappa I$ and $\lambda = \eta B$, where λ denotes the flux linkage per unit length and κ, $\eta > 0$ are geometry-dependent constants. The incremental inductance is then

$$L(I) = \frac{d\lambda}{dI} = L_{\mathrm{s}} + (L_0 - L_{\mathrm{s}})\,\mathrm{sech}^2(\beta I), \quad (4)$$

where

$$L_0 = \eta\kappa\mu_{\mathrm{i}}, \qquad L_{\mathrm{s}} = \eta\kappa\mu_{\mathrm{s}}, \qquad \beta = \kappa/H_*. \quad (5)$$

Consequently, $L(0) = L_0$ and

$$L(I) \to L_{\mathrm{s}} \text{ as } |I| \to \infty, \quad (6)$$

so that $L_{\mathrm{s}} \le L(I) \le L_0$. Integrating the incremental inductance with $\lambda(0) = 0$ gives

$$\lambda(I) = L_{\mathrm{s}} I + \frac{L_0 - L_{\mathrm{s}}}{\beta}\tanh(\beta I). \quad (7)$$

This constitutive law captures magnetic saturation while neglecting hysteresis, eddy-current effects, and magnetic memory, thereby retaining a minimal nonlinear benchmark model. A second nonlinearity is introduced through a distributed memoryless resistive shunt, representing an idealized current-limiting device. Such behavior is motivated by positive-temperature-coefficient resistive materials, whose resistance increases with temperature and which are used for thermal and overcurrent protection [4]. Neglecting the underlying thermal dynamics, we approximate the nonlinear voltage-current characteristic by

$$V = \mathcal{R}(i_{\mathrm{a}}), \qquad \mathcal{R}(i_{\mathrm{a}}) = R_{\mathrm{a}} i_{\mathrm{a}} + \gamma i_{\mathrm{a}}^3, \quad (8)$$

where $R_{\mathrm{a}} > 0$ and $\gamma \ge 0$ are constitutive parameters. The cubic term introduces an increasing effective resistance with current magnitude, while the memoryless approximation retains an algebraic constraint without additional dynamic states. The shunt is strictly monotone, since

$$\mathcal{R}'(i_{\mathrm{a}}) = R_{\mathrm{a}} + 3\gamma i_{\mathrm{a}}^2 > 0, \quad (9)$$

and dissipative, since its power loss per unit length satisfies

$$V i_{\mathrm{a}} = R_{\mathrm{a}} i_{\mathrm{a}}^2 + \gamma i_{\mathrm{a}}^4 \ge 0. \quad (10)$$

The resulting nonlinear transmission-line system

$$L(I)\partial_t I + \partial_x V + RI = 0, \quad (11a)$$

$$C\partial_t V + \partial_x I + GV + i_{\mathrm{a}} = 0, \quad (11b)$$

$$V - \mathcal{R}(i_{\mathrm{a}}) = 0 \quad (11c)$$

admits the nonlinear port-Hamiltonian descriptor representation

$$M(z)\partial_t z = (J - Q)z - N(z), \quad (12)$$

with state $z = (I, V, i_{\mathrm{a}})$, descriptor operator

$$M(z) = \begin{bmatrix} L(I) & 0 & 0 \\ 0 & C & 0 \\ 0 & 0 & 0 \end{bmatrix}, \quad (13)$$

energy-preserving interconnection operator

$$J = \begin{bmatrix} 0 & -\partial_x & 0 \\ -\partial_x & 0 & -1 \\ 0 & 1 & 0 \end{bmatrix}, \quad (14)$$

and linear and nonlinear dissipation contributions

$$Q = \begin{bmatrix} R & 0 & 0 \\ 0 & G & 0 \\ 0 & 0 & R_{\mathrm{a}} \end{bmatrix}, \qquad N(z) = \begin{bmatrix} 0 \\ 0 \\ \gamma i_{\mathrm{a}}^3 \end{bmatrix}. \quad (15)$$

The first two equations express the distributed voltage and current balances, while the third imposes the instantaneous nonlinear shunt characteristic. The state-dependent descriptor matrix $M(z)$ has constant rank two, while the interconnection operator J is formally skew-adjoint up to boundary contributions. The nonlinear dissipation satisfies

$$z^\top(Qz + N(z)) = RI^2 + GV^2 + R_{\mathrm{a}} i_{\mathrm{a}}^2 + \gamma i_{\mathrm{a}}^4 \ge 0. \quad (16)$$

The singular descriptor structure reflects the absence of energy storage in the nonlinear shunt, whose current is determined by the algebraic constraint. Consistent initial data must satisfy $i_{\mathrm{a}}(0, x) = \mathcal{R}^{-1}(V(0, x))$.

III. Index-One Structure

The regularity of the algebraic constraint is determined by the Jacobian of the nonlinear shunt characteristic. Due to (9), the algebraic constraint is regular, and the shunt characteristic is strictly monotone and globally invertible. Differentiating the algebraic constraint once with respect to time yields

$$\partial_t V - (R_{\mathrm{a}} + 3\gamma i_{\mathrm{a}}^2)\partial_t i_{\mathrm{a}} = 0. \quad (17)$$

Substituting the voltage evolution equation from the dynamical voltage equation gives

$$\partial_t i_{\mathrm{a}} = -\frac{\partial_x I + GV + i_{\mathrm{a}}}{C(R_{\mathrm{a}} + 3\gamma i_{\mathrm{a}}^2)}. \quad (18)$$

Since the denominator is strictly positive, a single differentiation of the algebraic constraint determines the algebraic time derivative. Thus, in the corresponding semi-explicit, spatially semidiscretized DAE sense [5], the system has differentiation index one. Equation (18) establishes the regularity of the algebraic dynamics.

IV. Exact Reduction to a Standard PDE

Strict positivity in (9) makes $\mathcal{R}$ strictly increasing on $\mathbb{R}$. Moreover,

$$\mathcal{R}(i_{\mathrm{a}}) \to \pm\infty \text{ as } i_{\mathrm{a}} \to \pm\infty, \quad (19)$$

so the inverse $f(V) = \mathcal{R}^{-1}(V)$ exists globally and is unique. For $\gamma > 0$, the cubic $\gamma i_{\mathrm{a}}^3 + R_{\mathrm{a}} i_{\mathrm{a}} - V = 0$ has discriminant

$$\Delta = \frac{V^2}{4\gamma^2} + \frac{R_{\mathrm{a}}^3}{27\gamma^3} > 0, \quad (20)$$

Preprint – Preprint – Preprint – Preprint – Preprint – Preprint

and the unique real root is given by Cardano's formula,

$$f(V) = \sqrt[3]{\frac{V}{2\gamma} + \sqrt{\Delta}} + \sqrt[3]{\frac{V}{2\gamma} - \sqrt{\Delta}}, \tag{21}$$

where real cube roots are understood. For $\gamma = 0$, it follows that $f(V) = V/R_\mathrm{a}$. Equivalently, for $\gamma > 0$, the inverse shunt characteristic $f(V)$ can be expressed in terms of hyperbolic functions, providing a numerically more stable alternative to Cardano's formula,

$$f(V) = 2\sqrt{\frac{R_\mathrm{a}}{3\gamma}} \sinh\left(\frac{1}{3}\operatorname{arsinh}\left(\frac{3V}{2R_\mathrm{a}}\sqrt{\frac{3\gamma}{R_\mathrm{a}}}\right)\right). \tag{22}$$

Substituting $i_\mathrm{a} = f(V)$ into the dynamical equations of (12) eliminates the algebraic variable, yielding the reduced system

$$\partial_t I = -\frac{\partial_x V + RI}{L(I)}, \tag{23a}$$

$$\partial_t V = -\frac{\partial_x I + GV + f(V)}{C}. \tag{23b}$$

This is an explicit, first-order, two-state quasilinear hyperbolic PDE system, providing an independent reference formulation for the benchmark. Its principal matrix and characteristic speeds are

$$A(I) = \begin{bmatrix} 0 & 1/L(I) \\ 1/C & 0 \end{bmatrix}, \quad c_\pm(I) = \pm\frac{1}{\sqrt{CL(I)}}. \tag{24}$$

Magnetic saturation decreases $L(I)$, increasing the magnitude of the characteristic speeds and enabling amplitude-dependent wave distortion. The PDE-DAE and reduced PDE formulations are equivalent for sufficiently regular solutions satisfying the initial algebraic constraint.

V. Energy Balance and Physical Consistency

Since L is the incremental inductance, the stored magnetic energy density is

$$W_\mathrm{m}(I) = \int_0^I sL(s)ds. \tag{25}$$

The Hamiltonian functional is defined by

$$\mathcal{H}(t) = \int_0^\ell \left[W_\mathrm{m}(I) + \frac{1}{2}CV^2\right] dx. \tag{26}$$

Its variational gradient satisfies

$$\frac{\delta\mathcal{H}}{\delta z} = M(z)^\top z, \tag{27}$$

establishing the energy-based interpretation of the descriptor formulation (12). Multiplying (12) by $z^\top$, integrating over the spatial domain, and using the formal skew-adjointness of J, yields

$$\begin{aligned}\frac{d\mathcal{H}}{dt} =& - I(t,\ell)V(t,\ell) + I(t,0)V(t,0) \\ & - \int_0^\ell \left[RI^2 + GV^2 + R_\mathrm{a} i_\mathrm{a}^2 + \gamma i_\mathrm{a}^4\right] dx.\end{aligned} \tag{28}$$

Equivalently, using $i_\mathrm{a} = f(V)$, the dissipation associated with the nonlinear shunt can be expressed as

$$Vf(V) = R_\mathrm{a} f(V)^2 + \gamma f(V)^4 \geq 0. \tag{29}$$

Thus, the algebraic reduction preserves the power-balance identity and passive dissipation, consistently with port-Hamiltonian energy-based modeling. For zero net boundary power, $d\mathcal{H}/dt \leq 0$. The memoryless shunt contributes to dissipation but not to energy storage. Equation (28) therefore provides an analytical reference for assessing passivity and energy consistency in both formulations and their numerical discretizations.

VI. Discretization and Results

A transmission line of length $\ell = 1$ m is partitioned into $N = 400$ uniform cells of width $\Delta x = \ell/N$. A staggered-grid discretization is employed, with currents I_j located at cell centers and voltages V_j and algebraic shunt currents $i_{\mathrm{a},j}$ at interior grid nodes. The resulting semidiscrete PDE-DAE system reads

$$L(I_j)\dot{I}_j + \frac{V_j - V_{j-1}}{\Delta x} + RI_j = 0, \tag{30a}$$

$$C\dot{V}_j + \frac{I_{j+1} - I_j}{\Delta x} + GV_j + i_{\mathrm{a},j} = 0, \tag{30b}$$

$$V_j - R_\mathrm{a} i_{\mathrm{a},j} - \gamma i_{\mathrm{a},j}^3 = 0, \tag{30c}$$

where the first equation holds for all $j \in \{1, \ldots, N\}$, and the remaining equations for all $j \in \{1, \ldots, N-1\}$. The staggered difference operators satisfy a discrete integration-by-parts identity, preserving the power-conserving interconnection structure up to boundary contributions. The transmission line is driven by a prescribed voltage source at the left boundary and terminated by a resistive load at the right boundary, that is,

$$V_0(t) = V_\mathrm{in}(t), \qquad V_N(t) = R_L I_N(t), \tag{31}$$

where $R_L = 25\ \Omega$ is the terminal load resistance. The input voltage is the compactly supported sine-squared pulse

$$V_\mathrm{in}(t) = \begin{cases} V_\mathrm{amp} \sin^2\left(\frac{\pi(t-t_\mathrm{s})}{t_\mathrm{e}-t_\mathrm{s}}\right), & t_\mathrm{s} \leq t \leq t_\mathrm{e}, \\ 0, & \text{otherwise}, \end{cases} \tag{32}$$

with amplitude $V_\mathrm{amp} = 80$ V, starting time $t_\mathrm{s} = 5$ μs, and ending time $t_\mathrm{e} = 9$ μs. The line is initially at rest, with $I_j(0) = V_j(0) = i_{\mathrm{a},j}(0) = 0$. The physical and constitutive parameters employed in the numerical experiments are summarized in Table I. The nonlinear shunt coefficient γ is selected so that the cubic contribution is half the linear contribution at a reference voltage of 80 V. The resulting index-one DAE is integrated using MATLAB's implicit solver `ode15i`, equipped with a sparse analytical Jacobian. For independent verification, the algebraic shunt currents and terminal voltage are eliminated analytically, and the equivalent reduced semidiscrete PDE is integrated using `ode15s`. For the reported simulation, both solvers employ a relative tolerance of 10^{-9} and a maximum time step of 10^{-8} s. The simulation covers $t \in [0, 80]$ μs, with numerical output sampled at intervals of 25 ns. The

Preprint – Preprint – Preprint – Preprint – Preprint – Preprint

TABLE I
PHYSICAL AND CONSTITUTIVE PARAMETERS

Parameter	Symbol	Value
Line length	ℓ	1 m
Series resistance	R	10^{-3} Ω/m
Shunt conductance	G	10^{-7} S/m
Capacitance	C	10^{-6} F/m
Initial inductance	L_0	10^{-3} H/m
Saturated inductance	L_s	2.5×10^{-4} H/m
Saturation parameter	β	1 A^{-1}
Linear shunt coefficient	R_a	500 Ωm
Cubic shunt coefficient	γ	2.1973×10^4 $\mathrm{V\,m^3/A^3}$
Terminal resistance	R_L	25 Ω

characteristic wave speeds range from $c_0 \approx 3.16 \times 10^4$ m/s in the unsaturated regime to $c_\mathrm{s} \approx 6.32 \times 10^4$ m/s under strong magnetic saturation. The corresponding amplitude-dependent propagation provides an analytical reference for assessing nonlinear wave behavior. For the considered discretization, the maximum absolute differences between the PDE-DAE and reduced PDE solutions are 3.65×10^{-4} A in current and 5.56×10^{-3} V in voltage, demonstrating close numerical agreement between the two mathematically equivalent formulations. To assess energy consistency, the discrete Hamiltonian is defined as

$$\mathcal{H}_h = \Delta x \sum_{j=1}^{N} W_m(I_j) + \frac{C\Delta x}{2} \sum_{j=1}^{N-1} V_j^2. \tag{33}$$

The spatial discretization satisfies the exact semidiscrete power-balance identity

$$\frac{d\mathcal{H}_h}{dt} = V_\mathrm{in} I_1 - R_L I_N^2 - D_h, \tag{34}$$

where the total distributed dissipation is

$$\begin{aligned} D_h = {} & R\Delta x \sum_{j=1}^{N} I_j^2 + G\Delta x \sum_{j=1}^{N-1} V_j^2 \\ & + \Delta x \sum_{j=1}^{N-1} V_j i_{\mathrm{a},j} \geq 0. \end{aligned} \tag{35}$$

Since the time integrators do not enforce the power balance exactly, the integrated energy-balance defect

$$\varepsilon_\mathcal{H}(t) = \mathcal{H}_h(t) - \mathcal{H}_h(0) - \int_0^t (P_{\partial,h} - D_h)\, ds \tag{36}$$

provides a measure of numerical energy consistency, where

$$P_{\partial,h} = V_\mathrm{in} I_1 - R_L I_N^2. \tag{37}$$

The benchmark thus provides complementary diagnostics for evaluating numerical methods, including agreement between the PDE-DAE and reduced PDE solutions, preservation of the nonlinear algebraic constraint, accuracy of wave propagation, and consistency with the port-Hamiltonian power balance.

Figure 2 illustrates the nonlinear current-wave propagation, the transient energy-balance defect, and the evolution of the discrete Hamiltonian. The maximum current reaches 9.22 A, driving the incremental inductance toward its saturation limit and increasing the local wave speed to 6.32×10^4 m/s. Furthermore, the maximum cubic-to-linear shunt ratio reaches 1.11, confirming the significant contribution of the nonlinear resistive shunt.

A pronounced decrease in the Hamiltonian is observed around $t = 26$ μs, coinciding with large negative boundary-power excursions. This behavior is consistent with the arrival of the nonlinear traveling wave at the resistive termination and the resulting energy extraction. Concurrently, the maximum cubic-to-linear shunt ratio decreases, indicating a weakening of the strongest local nonlinear shunt response. The integrated energy-balance defect exhibits transient oscillations during this rapid power-transfer event, potentially reflecting temporal integration and quadrature errors.

The numerical validation results are summarized in Table II. The PDE-DAE and reduced PDE formulations exhibit close agreement, with accurate satisfaction of the algebraic constraints. The maximum relative integrated energy-balance defect is 2.78×10^{-3}, while the Hamiltonian remains nonincreasing at the sampled times following the excitation pulse, consistently with the dissipative port-Hamiltonian structure. Finally, the reduced formulation achieves a computational speedup of approximately 14.4 for the considered implementation and solver settings.

TABLE II
NUMERICAL VALIDATION FOR $N = 400$ CELLS

Validation metric	Value
Algebraic constraints	
Max. shunt voltage residual	7.70×10^{-8} V
Max. load voltage residual	4.26×10^{-14} V
Max. inverse-shunt mismatch	9.39×10^{-11} A/m
Relative shunt residual	4.60×10^{-10}
Energy consistency	
Max. shunt power-law mismatch	3.25×10^{-11} W
Max. semidiscrete power residual	1.07×10^{-12} W
Max. integrated energy defect	1.22×10^{-6} J
Relative integrated energy defect	2.78×10^{-3}
Max. post-pulse energy increase	0 J
DAE-reduced PDE agreement	
Max. current difference	3.65×10^{-4} A
Max. voltage difference	5.56×10^{-3} V
Computational performance (Intel Core Ultra 5 225H×14, 32 GiB)	
`ode15i` execution time	135.58 s
`ode15s` execution time	9.41 s

VII. CONCLUSION

We presented a nonlinear transmission line as a compact benchmark for nonlinear port-Hamiltonian PDE-DAE systems and structure-preserving numerical methods. A reversible soft ferromagnetic B-H characteristic introduces a saturating incremental inductance, while a passive cubic resistive shunt gives rise to a regular index-one algebraic constraint. Exact elimination of the algebraic variable yields an equivalent two-state quasilinear PDE, providing a reference formulation for benchmarking PDE-DAE solvers. The analytical characteristic speeds and power-balance identity offer additional diagnostics

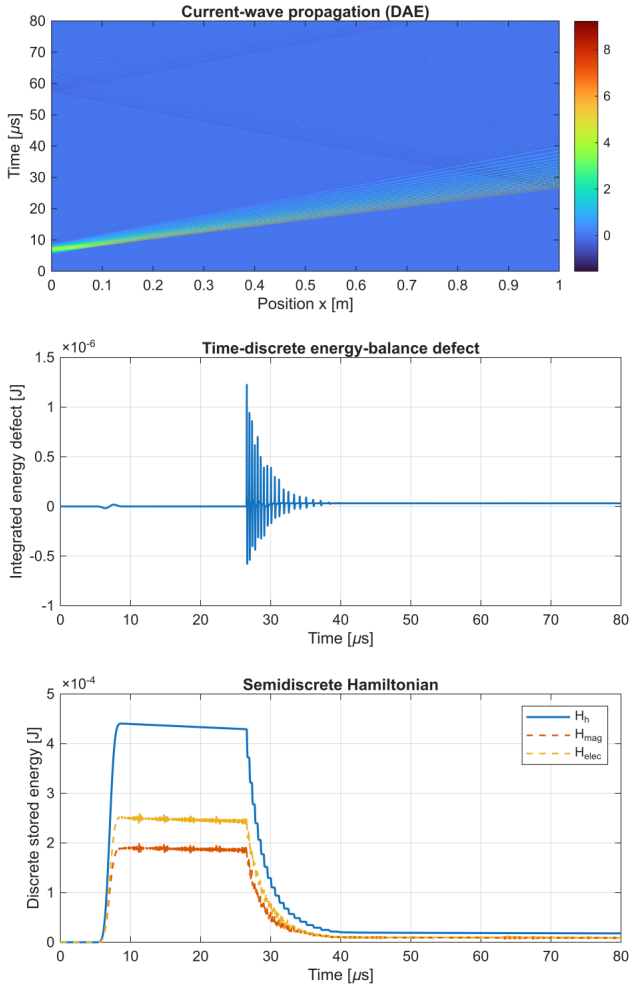


Fig. 2. Numerical benchmark simulation of the nonlinear transmission line model: (top) spatiotemporal current-wave propagation; (mid) time-discrete energy-balance defect, exhibiting transient oscillations during the wave-load interaction; (bot) evolution of the discrete Hamiltonian, showing a pronounced decrease as energy is extracted through the resistive termination. The Hamiltonian remains nonincreasing after the excitation pulse, consistent with the dissipative port-Hamiltonian structure.

for wave propagation accuracy, constraint preservation, and energy consistency. Extensions incorporating magnetic hysteresis and other memory effects are left for future investigation.

AKNOWLEDGEMENTS

This work was funded by the Deutsche Forschungsgemeinschaft (DFG, German Research Foundation) – Project-ID 531152215 – CRC 1701.

REFERENCES

[1] A. van der Schaft and D. Jeltsema, "Port-Hamiltonian systems theory: An introductory overview," *Found. Trends Syst. Control*, vol. 1, no. 2–3, pp. 173–378, 2014, doi: 10.1561/2600000002.

[2] D. M. Pozar, *Microwave Engineering*, 4th ed. Hoboken, NJ, USA: Wiley, 2012.

[3] G. Bertotti, *Hysteresis in Magnetism: For Physicists, Materials Scientists, and Engineers*. San Diego, CA, USA: Academic Press, 1998.

[4] A. Beauger and A. Lagrange, "Nonlinear temperature-dependent resistance for thermal protection using semiconductor ceramics," *Techniques de l'Ingénieur*, 2026, available online: https://www.techniques-ingenieur.fr/en/resources/article/ti589/semiconductor-ceramics-e2080

[5] P. Kunkel and V. Mehrmann, *Differential-Algebraic Equations: Analysis and Numerical Solution*. Zürich, Switzerland: European Mathematical Society, 2006, doi: 10.4171/017.

Preprint – Preprint – Preprint – Preprint – Preprint – Preprint